Theoretical predictions for the mechanical response of a model quartz crystal microbalance to two viscoelastic media: A thin sample layer and surrounding bath medium

Christopher C. White[a)] and John L. Schrag[b)]
Department of Chemistry and Rheology Research Center, University of Wisconsin, Madison, Wisconsin 53706

(Received 26 June 1998; accepted 7 September 1999)

Theoretical predictions are presented for the operating characteristics of a quartz crystal microbalance (QCM) system consisting of the crystal, an attached viscoelastic sample layer, and a surrounding viscoelastic bath medium. Predictions are given for the spatial variation of ''particle'' velocity and velocity gradient throughout the sample layer, for the characteristic mechanical impedance acting on the crystal surface due to the viscoelastic sample layer plus surrounding bath medium, and for the resultant changes, Δf_r, in the resonance frequency of the QCM. Errors introduced by employing the usual simple Sauerbrey-type Δf_r/sample-layer–mass relationship, together with a constant frequency offset to approximate the effect of the viscoelastic bath medium, are explored. In general, the viscoelastic properties of both the sample and bath media can substantially affect the apparent thickness (mass) of the sample layer if it is obtained by employing the typical Sauerbrey-type approximation noted above. © *1999 American Institute of Physics.* [S0021-9606(99)50845-3]

INTRODUCTION

In many studies, measurement of very small sample masses is necessary. Knife edge or electronic balances can readily achieve a sensitivity of about 0.01 mg while electrostatic balances have a typical sensitivity of 0.15 μg and probably represent the state-of-the-art in commercial instruments for direct mass determination. Rapid advances in fields such as surface science, microelectronics, and thin film technologies have made the ability to measure even smaller masses of critical importance.

Quartz crystal microbalances (QCMs), developed in the late 1950's and early 1960's, appear to fulfill these mass measurement needs at least for some samples; nominal pg detection limits have been reported.[1] These devices have three attractive features: high measurement precision (at least 1 part in 10^6 for resonance frequency), temporal stability of the resonator (ppb for weeks), and relatively low cost. However, QCMs do not DIRECTLY measure mass. With a quartz crystal microbalance system, the mass of a thin sample layer attached to the surface of a QCM is INFERRED from the resultant change, Δf_r, in resonance frequency, f_r, from that of the bare quartz resonator, f_r^0, due to the influence of the sample. If the applied layer is firmly attached and rigid (motion within the layer is spatially constant in both amplitude and phase), the change in resonance frequency can be directly related to sample mass. Recently, QCMs oscillating in simple shear have shown high mechanical Qs even when immersed in liquids or other mechanically lossy media.[2–29] The effect of a surrounding lossy medium on the resonance frequency of a bare QCM has been theoretically predicted[10,11] and experimentally verified[29] (very low viscosity media) to be approximately equivalent to a constant frequency offset from the resonance frequency seen when no surrounding medium is present. This has led to a great expansion of applications in which the QCM has been employed. Quite often in these new applications a QCM with an applied viscoelastic sample layer, the mass or thickness of which is to be determined, is immersed in a surrounding viscous or viscoelastic medium. Theoretical predictions for this situation have not been presented. Thus for QCMs as currently employed, there are several questions that have not been addressed. For example, under what conditions are simple $\Delta f/\text{sample mass}$ (Sauerbrey-type)[30,31] relationships applicable? How is the behavior of a viscoelastic sample layer and the QCM resonance frequency affected by the presence of a second surrounding viscoelastic bath medium? What is the relationship between what is physically occurring in the sample layer and the change in resonance frequency that is being sensed? In this article, theoretical predictions are presented for the spatial variation of the velocity and velocity gradient throughout the sample layer, the characteristic mechanical impedance at the crystal surface due to the presence of the viscoelastic sample layer plus a surrounding viscoelastic bath medium, and the resultant changes in QCM resonance frequency obtained by employing a simple harmonic oscillator approximation to the quartz resonator together with the characteristic impedance due to the attached sample layer and surrounding medium. Predictions are presented for selected cases to illustrate the link between what is occurring in the sample layer and surrounding medium and changes in the QCM resonance frequency.

At this point it is important to note that previous theoretical treatments, as well as the one presented here, have idealized the quartz crystal resonator motional behavior by

[a)]Present address: NIST, Bldg. 226, Rm. B350, Gaithersburg, Maryland 20899.
[b)]Author to whom correspondence should be addressed.

 © 1999 American Institute of Physics

Downloaded 19 Apr 2002 to 129.6.104.125. Redistribution subject to AIP license or copyright, see http://ojps.aip.org/jcpo/jcpcr.jsp

assuming only an in-plane motion of the surface of the quartz crystal so that only simple shear waves propagate away from its surface. Recent experimental evidence has confirmed that, in addition to shear waves, a longitudinal wave component is also usually produced by the actual motion of quartz crystals[32] as noted years ago by Jaffe.[33–36] If one is attempting to determine the viscoelastic properties of the sample layer, the presence of a longitudinal wave component propagating in the sample and surrounding bath medium will usually considerably increase the difficulty of interpreting the data.

BACKGROUND

Excellent descriptions of the historical development of the QCM are in the literature,[20,37] so only a brief overview is presented here. Cady[34] apparently developed the first piezoelectric resonator in 1918. In 1957 Onoe[38] considered the problem of a quartz plate loaded by a rigid surface film of metal and predicted the experimentally observed frequency shifts; this is the first description of a device similar to the modern quartz crystal microbalance.

Sauerbrey,[30,31] first in 1957 and later in 1959, published pioneering articles which provided a description and experimental verification of the mass/frequency shift relation for rigid foreign layers firmly attached to the surface of a resonator; this derivation implicitly assumes that a deposited thin layer of foreign material (mass m_f) is at the antinode of the standing wave in the quartz crystal and that its density and shear modulus are such that it can be treated approximately as an extension of the quartz crystal. [The mass of the foreign material (m_f) attached to the surface of the crystal would be equivalent to an increase in the mass of the crystal (Δm_q)]. Thus the frequency change was calculated as though it was simply the result of an increase in the thickness of the crystal.

$$\Delta f_r = \left[\frac{-2f_{r0}^2}{A\sqrt{\rho_q G_q}}\right]\Delta m_q, \tag{1}$$

where Δf_r is the change in resonance frequency due to the added mass; f_{r0} is the resonance frequency of the unloaded resonator; ρ_q and G_q are the density and shear modulus of quartz, respectively; and A is the surface area of the resonator. From this relation the sensitivity of the QCM was predicted and subsequently experimentally verified to be $\approx 10^{-12}$ g.[1] This treatment is rigorously valid only for infinitesimally thin films that have an acoustic impedance (for shear waves) close to that of quartz, conditions that are approximated well by fairly rigid, firmly attached thin films.

There have been several extensions of Sauerbrey's pioneering work including more realistic descriptions of the influence of the sample layer, such as incorporation of the effects of shear waves propagating in the attached sample medium and thus the inclusion of its mechanical properties. Working equations have been obtained for the following cases: the crystal and attached rigid layer (Stockbridge),[39] crystal immersed in a viscous medium of infinite extent (Kanazawa),[10,11] and crystal and attached viscoelastic layer (Miller,[40] Benes,[41,42] Johannsmann,[13] Kanazawa,[14] Nwankwo[43]). An important case for which no predictions are available to date is that of the crystal with attached viscoelastic sample layer immersed in a second viscoelastic bath medium. The influence of the surrounding medium is evident when the QCM is used in liquid systems; the combination of a viscoelastic sample layer plus surrounding viscoelastic bath medium can exhibit even more complex behavior. At typical QCM operating frequencies, many liquids are viscoelastic.

There have been treatments of the QCM with an attached layer that employ electroacoustic analogies together with transmission line theory.[44] There also is a treatment of the electrical behavior of a layered piezoelectric resonator.[41] These approaches led to formal solutions that in principle could be applied to the cases considered here, but interpretation of the results is complicated.

This article presents a rigorous derivation of the characteristic mechanical impedance acting on a quartz resonator (simple shear deformation) due to an attached viscoelastic sample layer and a surrounding viscoelastic bath medium which enables quantitative evaluations of the various simplifications and approximations employed previously in the analysis of QCM data. This impedance, together with a simple harmonic oscillator approximation of a quartz resonator, is used to examine QCM resonance frequency behavior as a function of the viscoelastic properties of sample and surrounding media to determine the conditions under which resonance frequency shifts, together with the usual simple analysis approaches, can and cannot provide sample mass determinations. The included theoretical predictions for the spatial variation of the velocity and velocity gradient throughout the sample layer show the origins of the eventual failure of simple Δf/mass relationships.

SPATIAL VARIATION OF VELOCITY AND VELOCITY GRADIENT

Since the crystal-induced strains in the sample are generally very small, the analysis presented here assumes that the sample layer and the surrounding medium exhibit linear viscoelastic behavior.[5,7,45] For steady-state, sinusoidally time-varying simple shearing deformations, either medium is describable in terms of its density and either its complex shear modulus G^* or its complex viscosity η^*.

$$\begin{aligned} G^* &= G' + iG'' = G_M e^{+i\delta}, \\ \eta^* &= \frac{G^*}{i\omega} = \eta' - i\eta'' = \eta_M e^{-i\phi}, \end{aligned} \tag{2}$$

where G' or η'' describe energy storage and G'' or η' describe energy dissipation in the media. Time varying shearing deformations of viscoelastic media give rise to propagating shear waves. For freely propagating sinusoidally time varying plane shear waves, the medium displacement ξ is of the form $\xi = \xi_M e^{i(\omega t \pm \gamma x)}$ where γ is the complex wave propagation factor which is related to the viscoelastic properties and density of the medium in which the waves are traveling.[46–48]

$$\gamma = (\beta - i\alpha) = \left(\frac{-i\omega\rho}{\eta^*}\right)^{1/2}, \tag{3}$$

Downloaded 19 Apr 2002 to 129.6.104.125. Redistribution subject to AIP license or copyright, see http://ojps.aip.org/jcpo/jcpcr.jsp

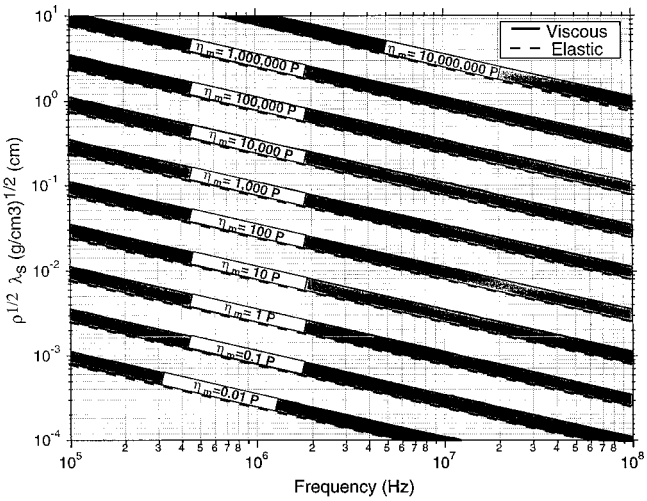

FIG. 1. $\rho^{1/2}\lambda_s$ vs. f for plane shear waves as a function of the viscoelastic properties of the medium. Solid line: Purely viscous limit; dashed line: purely elastic limit; gray area corresponds to values of ϕ between 0° and 90°.

where ω is the radian frequency and ρ the density. β is related to the shear wavelength λ_s and α specifies the spatial attenuation of the wave.[46–48]

$$\beta=\frac{2\pi}{\lambda_s}=\sqrt{\frac{\omega\rho}{\eta_M}}\cos[(\pi/4)-(\phi/2)], \tag{4}$$

$$\alpha=\sqrt{\frac{\omega\rho}{\eta_M}}\sin[(\pi/4)-(\phi/2)]. \tag{5}$$

The angle ϕ of the complex viscosity is readily specified in terms of α and β ($\tan\phi=(\eta''/\eta')=[(\beta/\alpha)-(\alpha/\beta)]/2$, or $\tan(\delta/2)=\alpha/\beta$).[46,47,49] Thus, for a perfectly viscous medium ($\phi=0°$), $\alpha=\beta$; for a perfectly elastic material ($\phi=90°$), $\alpha=0$. For convenience when assessing QCM behavior in the following sections, Fig. 1 presents a plot of $\rho^{1/2}\lambda_s$ vs. frequency for a wide range of viscoelastic properties so that values of λ_s can be readily estimated.

The two-media case being considered here is illustrated in Fig. 2. A driving surface at $x=-D$ represents the crystal surface of a QCM in contact with the sample layer; the interface between the sample and the surrounding viscoelastic medium is at $x=0$. Thus, medium 1 (sample layer) has a thickness D while medium 2 is assumed to be effectively infinite in extent in the $+x$ direction. Steady state conditions are assumed; the velocity of the driving surface at $x=-D$ is taken to be

$$\dot{\xi}^*_{ds}=\dot{\xi}_0 e^{i\omega t}, \tag{6}$$

where $\dot{\xi}^*_{ds}$ is in the y direction. For a sufficiently large driving surface area this will, in general, lead to plane shear waves propagating in these media. Initially, the moving driving surface would produce a plane shear wave propagating in the $+x$ direction; the interface between the two media at $x=0$ would then give rise to a reflected wave traveling in the $-x$ direction in medium 1 and a transmitted wave propagating ($+x$ direction) in medium 2. Many repetitions of this at $x=0$, and subsequent reflections at $x=-D$, lead to a resultant steady-state wave field that can be represented in terms of three waves A, B, and C, as shown. The A wave represents the sum of all waves propagating in the $+x$ direction in medium 1; the B wave, the sum of all waves propagating in the $-x$ direction in the same medium. The C wave represents the sum of all waves propagating in the $+x$ direction in medium 2 (no reflected waves). Shear waves generally show rapid spatial attenuation except in highly elastic media; thus the assumption of no reflected waves in medium 2 from sample container walls is generally an excellent approximation at QCM frequencies even for small containers. (In water, 5 MHz shear waves attenuate by a factor of 2.9×10^5 in a distance of 8 μm.) In the following, all parameters that relate to medium 1 or medium 2 carry the subscript 1 or 2, respectively.

The spatial variation of the velocity $\dot{\xi}^*$ in medium 1 is given by:

$$\dot{\xi}^*=\overline{A}e^{+i(\omega t-\gamma_1 x)}+\overline{B}e^{+i(\omega t+\gamma_1 x)} \quad \text{for} \quad -D\leqslant x\leqslant 0, \tag{7}$$

and in medium 2 by

$$\dot{\xi}^*=\overline{C}e^{+i(\omega t-\gamma_2 x)} \quad \text{for} \quad x\geqslant 0, \tag{8}$$

where the amplitude coefficients $\overline{A},\overline{B},\overline{C}$ are, in general, complex, as are the propagation coefficients γ_i. The shear rate $\dot{\gamma}^*_{xy}$ is given by[50]

$$\dot{\gamma}^*_{xy}=\left(\frac{\partial\dot{\xi}_y}{\partial x}+\frac{\partial\dot{\xi}_x}{\partial y}\right). \tag{9}$$

However, since $\dot{\xi}$ has only a y component, the shear rate and the velocity gradient g^* (x direction) are identical ($\dot{\gamma}^*_{xy}=\partial\dot{\xi}_y/\partial x=g^*$). Thus, from here on, g^* is used in place of $\dot{\gamma}^*_{xy}$ to simplify notation (all γ's will be complex propagation coefficients). The unspecified coefficients $\overline{A}$, $\overline{B}$, and $\overline{C}$ are evaluated by employing appropriate boundary conditions (see Appendix). The resulting expressions for $\dot{\xi}^*$ and g^* in media 1 and 2 are:

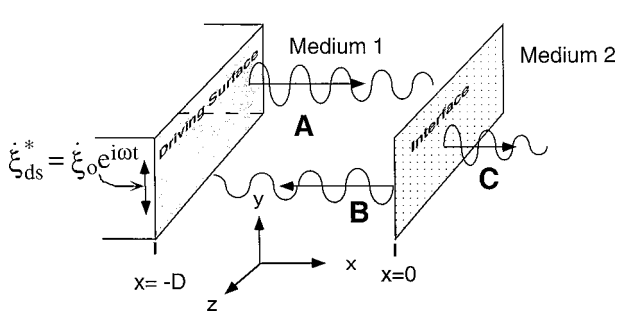

FIG. 2. Model system for which velocity and velocity gradient spatial profiles in the sample layer and surrounding medium and the characteristic impedance (at $x=-D$) have been obtained.

Downloaded 19 Apr 2002 to 129.6.104.125. Redistribution subject to AIP license or copyright, see http://ojps.aip.org/jcpo/jcpcr.jsp

TABLE I. Three categories of thin sample layer/surrounding bath media illustrating three distinct applications regimes for quartz crystal microbalances (frequencies assumed to be in the range from 5×10^5 to 5×10^6 Hz.)[a]

Sample layer	Bath medium	η_{1M} (Poise)	η_{2M} (Poise)	$\frac{\alpha_1}{\beta_1}$	$\frac{\alpha_2}{\beta_2}$	approx. β_1/β_2	Comments on Evaluation of Sample Layer Thickness
Thin metal layer	air or vacuum	$\geqslant10^4$	$\cong2\times10^{-4}$	$\leqslant0.001$	1	0.01 to 0.5	Simple Sauerbrey analysis applies unless sample layer thickness is very small. Although β_1/β_2 is large, X_m^s from bath is very small since ρ_2 is $\leqslant0.001$ g/cm^3 [see Eq. (27)].
Thin metal layer	water	$\geqslant10^4$	0.01	$\leqslant0.001$	1	$\leqslant0.005$	Sauerbrey type analysis usually applies unless sample layer is very thin, in which case medium 2 contribution usually can be treated as additive (see summary), but each case should be evaluated carefully.
Thin glassy polymer layer	water	$\geqslant5\times10^2$	0.01	$\leqslant0.02$	1	$\leqslant0.008$	
Thin rubbery polymer layer	water	$\geqslant2$	0.01	$\geqslant0.5$	1	$\leqslant0.1$	Significant deviation from simple Sauerbrey type behavior is common. Full impedance treatment is usually necessary.

[a]References 45, 53, 54.

medium 1:

$$\dot{\xi}^*=\frac{\dot{\xi}_0[P-iQ]}{[E+iF]}e^{i\omega t}$$
$$=\frac{\dot{\xi}_0[P^2+Q^2]^{1/2}}{[E^2+F^2]^{1/2}}e^{i[\omega t-\tan^{-1}(Q/P)-\tan^{-1}(F/E)]}$$
$$\text{for } -D\leqslant x\leqslant 0, \tag{10}$$

and

$$g^*=-\frac{\dot{\xi}_0\gamma_1[K+iL]e^{i\omega t}}{E+iF}$$
$$=\frac{\dot{\xi}_0\beta_1[1+(\alpha_1/\beta_1)^2]^{1/2}[K^2+L^2]^{1/2}}{[E^2+F^2]^{1/2}}$$
$$\times e^{i[\omega t-\pi/2-\tan^{-1}(\alpha_1/\beta_1)-\tan^{-1}(L/K)-\tan^{-1}(F/E)]}$$
$$\text{for } -D\leqslant x\leqslant 0; \tag{11}$$

medium 2:

$$\dot{\xi}^*=\frac{\dot{\xi}_0[J+iN]}{[E+iF]}e^{i\omega t}$$
$$=\frac{\dot{\xi}_0[J^2+N^2]^{1/2}}{[E^2+F^2]^{1/2}}e^{i[\omega t+\tan^{-1}(N/J)-\tan^{-1}(F/E)]}$$
$$\text{for } x\geqslant 0, \tag{12}$$

and

$$g^*=\frac{\dot{\xi}_0\gamma_2[J+iN]e^{i\omega t}}{[E+iF]}$$
$$=\frac{\dot{\xi}_0\beta_1[1+(\alpha_1/\beta_1)^2]^{1/2}[J^2+N^2]^{1/2}}{[E^2+F^2]^{1/2}}$$
$$\times e^{i[\omega t+(\pi/2)-\tan^{-1}(\alpha_1/\beta_1)+\tan^{-1}(N/J)-\tan^{-1}(F/E)]}$$
$$\text{for } x\geqslant 0, \tag{13}$$

where E,F,J,K,L,N,P, and Q are defined in the Appendix. For graphical simplicity, the spatial variation of a normalized velocity is examined when exploring the spatial motional variation in the sample layer.

$$\frac{\dot{\xi}^*}{(\dot{\xi}^*)_{x=-D}}=\frac{\dot{\xi}^*}{\dot{\xi}_0e^{i\omega t}}$$
$$=\frac{[P^2+Q^2]^{1/2}}{[E^2+F^2]^{1/2}}e^{i[-\tan^{-1}(Q/P)-\tan^{-1}(F/E)]}$$
$$=Me^{i\Psi}\quad\text{for } -D\leqslant x\leqslant 0. \tag{14}$$

Three basic categories of sample layer/surrounding bath medium have been selected to illustrate distinct behaviors typically seen in many QCM applications: metal sample layer/water, glassy polymer sample layer/water, and rubbery polymer sample layer/water. Table I lists typical material parameter ranges for these cases. Also shown are brief summary comments on analysis approaches needed for these cases. The influence of viscoelastic bath media is addressed later.

Illustrations of the spatial variation of M and Ψ in layer 1 are shown in Fig. 3 for an unusual metal layer/water case with sample layer thickness $\beta_1D=1$ (β_1D specifies thickness in units of wavelength, a reduced variable format that eliminates the need to specify η_{1M} of layer 1) which corresponds to a layer perhaps ten times thicker than is typically encountered ($D\cong0.16\lambda_S$). The influence of the surrounding medium is specified by β_1/β_2 (ratio of the shear wavelengths for the two media): 0.001 corresponds to a worst case metal layer/water interface (η_{1M}/ρ_1 only 10^6 times larger than η_{2M}/ρ_2). These values of β_1D and β_1/β_2 were chosen to represent a worst case extreme; note that medium 2 is purely viscous. (A typical thin layer of metal on a QCM surrounded by air would correspond to $\beta_1D\leqslant0.01$ and $\beta_1/\beta_2\leqslant0.000\,01$. An extracellular polymer produced by bacteria and adsorbed onto the surface of a QCM probably corresponds to $\beta_1D\leqslant1$ and $\beta_1/\beta_2\leqslant0.1$.) If the sample

Downloaded 19 Apr 2002 to 129.6.104.125. Redistribution subject to AIP license or copyright, see http://ojps.aip.org/jcpo/jcpcr.jsp

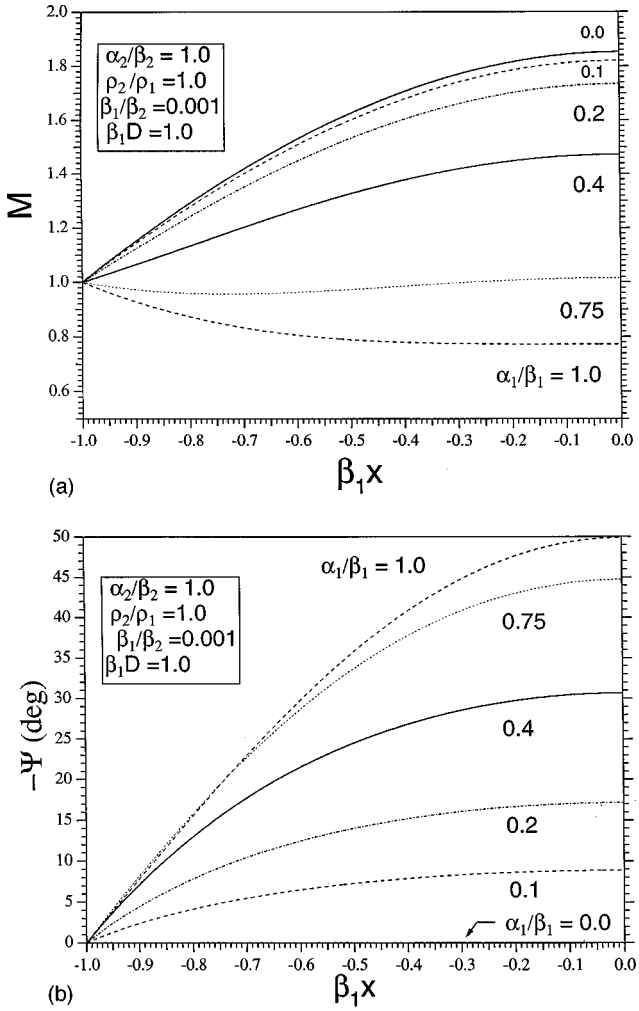

FIG. 3. (a) Magnitude (M) of normalized velocity vs. reduced variable position ($\beta_1 X$) in thick sample layer in contact with purely viscous second (bath) medium of much lower viscosity ($\eta_{1M}/\eta_{2M}=10^6$). Moving surface at $\beta_1 x=-1$; interface between two media at $\beta_1 x=0$. (b) Relative phasing (Ψ) of normalized velocity vs. reduced variable position $\beta_1 x$ in thick sample layer in contact with purely viscous second bath medium of much lower viscosity ($\eta_{1M}/\eta_{2M}=10^6$). Moving surface at $\beta_1 x=-1$; interface between two media at $\beta_1 x=0$.

layer (layer 1) were behaving like a perfectly rigid material, M would equal 1 and Ψ would equal 0° throughout layer 1. The left side of the plots ($-\beta_1 x=\beta_1 D$) corresponds to the QCM driving surface, and the right side of the plot ($\beta_1 x=0$) to the interface between medium 1 and medium 2. For this layer thickness, M varies substantially; it can be greater or less than one depending on the viscoelastic character of the layer. Note that since $\tan\phi=[(\beta_1/\alpha_1)-(\alpha_1/\beta_1)]/2$ or $\tan(\delta/2)=(\alpha_1/\beta_1)$, the quantity α_i/β_i can be thought of as a ''viscoelastic ratio'' for medium i. Clearly medium 1 is not approximating rigid layer behavior. The angle Ψ shows up to a 50° shift for a purely viscous sample layer ($\alpha_1/\beta_1=1$), and even for a highly elastic layer ($\alpha_1/\beta_1=0.01$, not shown) there is still a 1° shift. Thus, for thick layers, assuming rigid sample layer behavior frequently will introduce considerable error. For more typical applications of the QCM ($\beta_1 D=0.1$, $\beta_1/\beta_2=0.001$), M varies by 0.52% at most throughout the sample, while Ψ varies by 0.6° at most, closely approximating rigid layer behavior. If the two media are closer in mechanical properties ($\beta_1/\beta_2=0.1$, $\beta_1 D=0.1$), M varies by up to 1% throughout the sample and Ψ varies by up to 1.2°, showing a small but now significant influence of the second layer. Thus, as shown later, when the applied layer 1 is thin ($\beta_1 D\leqslant 0.1$ corresponding to $D\leqslant 0.0159\lambda_1$), and the difference in mechanical properties between layer 1 and layer 2 is large ($\beta_1/\beta_2\leqslant 0.001$), the application of simple Sauerbrey-type expressions relating the change in layer thickness to change in resonance frequency can be employed with minimal error. As the layer thickness becomes larger, there will be significant deviations from rigid layer behavior, and differences in the viscoelastic nature of the sample layer can result in dramatically different spatial variations of the reduced velocity. (The velocity distribution within a sample layer probably cannot be experimentally determined for a typical QCM.)

MECHANICAL IMPEDANCE AT THE DRIVING SURFACE

The velocity and velocity gradient expressions presented above reflect actual motions in the sample layer. The effect of these motions is to exert forces on the driving surface which lead to the changes in resonance frequency usually monitored for QCMs. A particularly convenient way to examine these effects is to consider the mechanical impedance at the driving surface of the QCM due to the presence of media 1 and 2; this impedance is affected by the spatial variation of motion in the sample layer and in the second medium. In contrast to the spatial distribution of the velocity and velocity gradient in the sample layer, this impedance can be determined experimentally. (Recall that for an ideal moving mass the mechanical impedance $Z_M=R_M+iX_M$ would be $Z_M=iX_M=i\omega M$.)

The effect of layer 1 and the surrounding bath medium (layer 2) on QCM behavior is conveniently explored in terms of the complex characteristic impedance $Z_m^s=R_m^s+iX_m^s$ (impedance per unit area). For the experimental configuration of Fig. 2, the characteristic impedance acting on the driving surface is given by

$$Z_m^s=-\left.\frac{\eta_1^* g^*}{\dot{\xi}^*}\right|_{x=-D}. \tag{15}$$

Substitution of Eqs. (10) and (11) into (15) yields

$$Z_m^s=-\frac{\eta_1^*\gamma_1[K+iL]}{[Q+iP]}, \tag{16}$$

from which

$$R_m^s=|Z_m^s|\cos\left[-\phi_1-\tan^{-1}\left(\frac{\alpha_1}{\beta_1}\right)+\tan^{-1}\left(\frac{L}{K}\right)-\tan^{-1}\left(\frac{Q}{P}\right)\right], \tag{17}$$

and

$$X_m^s=|Z_m^s|\sin\left[-\phi_1-\tan^{-1}\left(\frac{\alpha_1}{\beta_1}\right)+\tan^{-1}\left(\frac{L}{K}\right)-\tan^{-1}\left(\frac{Q}{P}\right)\right], \tag{18}$$

Downloaded 19 Apr 2002 to 129.6.104.125. Redistribution subject to AIP license or copyright, see http://ojps.aip.org/jcpo/jcpcr.jsp

where

$$|Z_m^s| = \frac{\eta_{1M}\beta_1[1+(\alpha_1/\beta_1)^2]^{1/2}[K^2+L^2]^{1/2}}{[P^2+Q^2]^{1/2}}. \tag{19}$$

These equations reduce to known expressions for specific cases: the general case of gap width D where the driving surface is at $x=-D$ and a fixed reflector is at $x=0$,[51,46] and two limiting cases of this configuration that are frequently used in rheological instruments: the ''gap loading'' limit for which the gap width is infinitesimal,[46,45] and the ''surface loading'' limit for which the gap width is effectively infinite (driving surface at $x=-D$ but effectively no reflecting surface).[51,45,52] The details of these comparisons are presented elsewhere.[33]

To obtain a universal plot format, a reduced characteristic mechanical impedance $(Z_m^s)_N$ has been obtained by dividing the characteristic mechanical impedance [Eq. (16)] by $\sqrt{\omega\rho_1\eta_{1M}}$ so that there is no need to specify the magnitude of the complex viscosity or density of the sample layer or the working frequency of the specific experimental setup being considered. $(\eta_{1M}\beta_1[1+(\alpha_1/\beta_1)^2]^{1/2}e^{-i[\phi_1+\tan^{-1}(\alpha_1/\beta_1)]} = \sqrt{\omega\rho_1\eta_{1M}}e^{-i[(\phi_1/2)+(\pi/4)]}$.) The components of the reduced characteristic impedance are given by

$$(R_m^s)_N = \frac{[K^2+L^2]^{1/2}}{[P^2+Q^2]^{1/2}} \times \cos\left[-\frac{\phi_1}{2}-\frac{\pi}{4}+\tan^{-1}\left(\frac{L}{K}\right)-\tan^{-1}\left(\frac{Q}{P}\right)\right], \tag{20}$$

$$(X_m^s)_N = \frac{[K^2+L^2]^{1/2}}{[P^2+Q^2]^{1/2}} \times \sin\left[-\frac{\phi_1}{2}-\frac{\pi}{4}+\tan^{-1}\left(\frac{L}{K}\right)-\tan^{-1}\left(\frac{Q}{P}\right)\right]. \tag{21}$$

These reduced real and imaginary impedance components have been examined for a variety of conditions.

Three different ways of examining characteristic impedance predictions have been explored. The first is presented here; the other two are described and observations noted, but the details are presented elsewhere.[33] In the first approach, reduced characteristic impedance components are examined as a function of layer 1 thickness, again expressed in terms of $\beta_1 D$; Figs. 4 and 5 show results for two ranges of $\beta_1 D$ ($\beta_1 D \leqslant 2.0$ and $\beta_1 D \leqslant 0.3$) representing ranges for thick and thin sample layers. A second approach is to evaluate the characteristic impedance divided by the characteristic impedance if only layer 1 were present; this format sensitively reflects changes due to the presence of the surrounding bath medium (''layer 2''). A third approach is to evaluate the characteristic impedance divided by the characteristic impedance if only the bath medium were present; this format is particularly sensitive to the changes due to the presence of the attached sample (layer 1).

Predicted values of the real $(R_m^s)_N$ and imaginary $(X_m^s)_N$ components of the reduced characteristic mechanical impedance versus sample layer thickness when a purely viscous second bath medium is present are shown in Figs. 4 and 5; the different curves are for different values of α_1/β_1 and thus reflect changes caused by changes in the ''viscoelastic ratio'' for medium 1. The effect of the second medium is

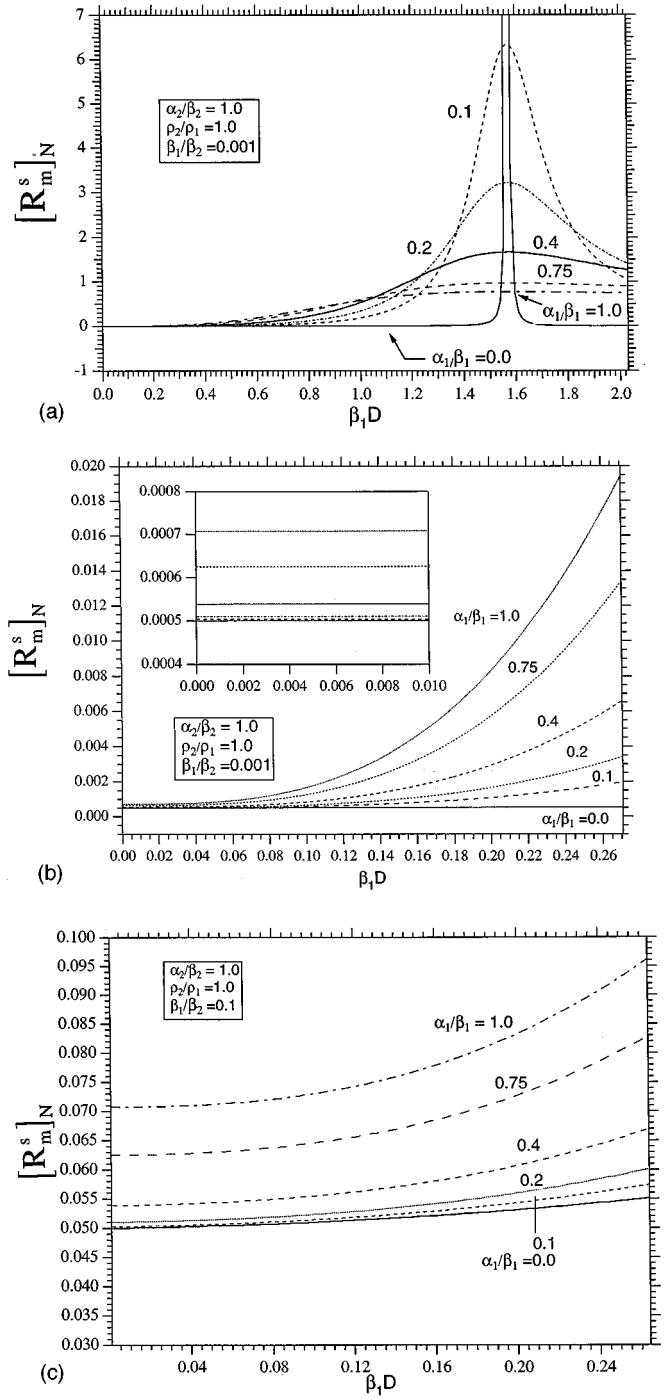

FIG. 4. (a) Real part $(R_m^s)_N$ of the reduced characteristic mechanical impedance at the drive surface ($x=-D$) vs. $\beta_1 D$ for various values of the ''viscoelastic ratio'' α_1/β_1 for a large range of sample layer thickness; second medium purely viscous with $\eta_{1M}/\eta_{2M}=10^6$ (second medium contribution small). (b) $(R_m^s)_N$ at $x=-D$ vs. $\beta_1 D$ for various values of α_1/β_1 for a small range of sample layer thickness; second medium purely viscous with $\eta_{1M}/\eta_{2M}=10^6$ (second medium contribution small). Inset shows thin layer region of plot. (c) $(R_m^s)_N$ at $x=-D$ vs. $\beta_1 D$ for various values of α_1/β_1 for a small range of sample layer thickness; second medium purely viscous with $\eta_{1M}/\eta_{2M}=10^2$ (second medium contribution substantial).

Downloaded 19 Apr 2002 to 129.6.104.125. Redistribution subject to AIP license or copyright, see http://ojps.aip.org/jcpo/jcpcr.jsp

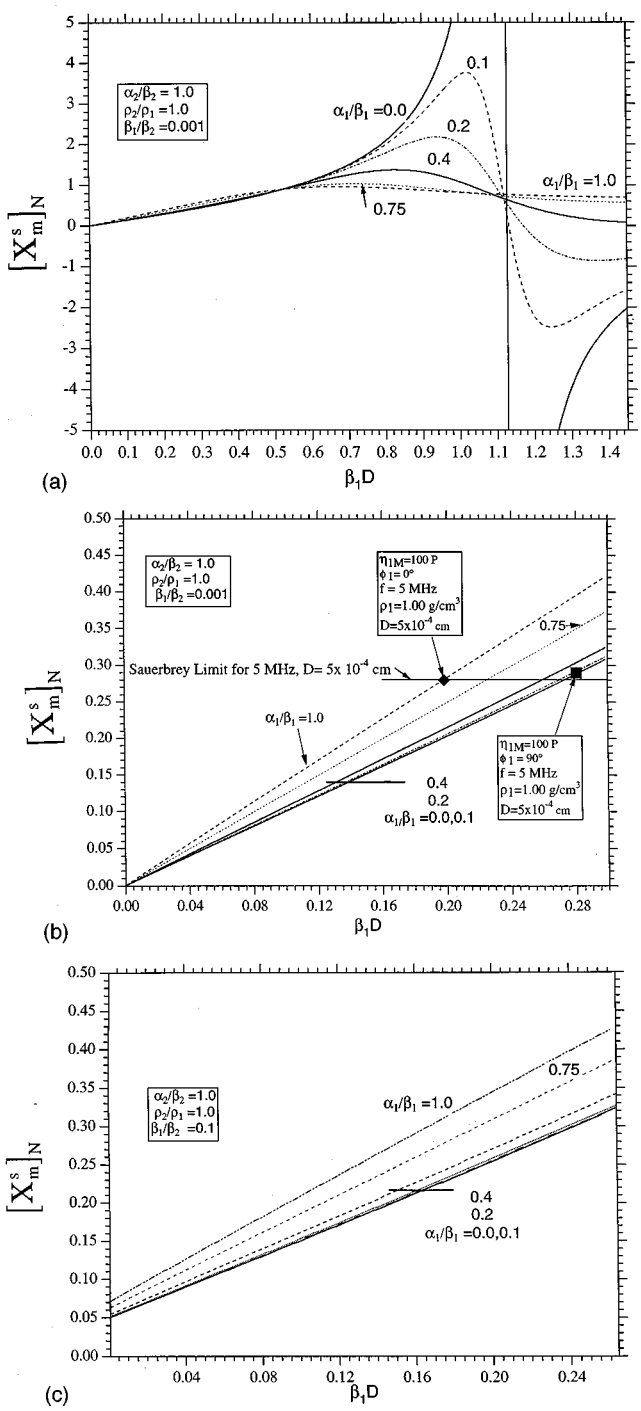

FIG. 5. (a) Imaginary part $(X_m^s)_N$ of the reduced characteristic mechanical impedance at the drive surface $x=-D$ vs. $\beta_1 D$ for various values of the ''viscoelastic ratio'' α_1/β_1 for a large range of sample layer thickness; second medium purely viscous with $\eta_{1M}/\eta_{2M}=10^6$ (second medium contribution small). (b) $(X_m^s)_N$ at $x=-D$ vs. $\beta_1 D$ for various values of α_1/β_1 for a small range of sample layer thickness; second medium purely viscous with $\eta_{1M}/\eta_{2M}=10^6$ (second medium contribution small). Also included are two points for specific layer 1 thickness and material properties values (see text). (c) $(X_m^s)_N$ at $x=-D$ vs. $\beta_1 D$ for various values of α_1/β_1 for a small range of sample layer thickness; second medium purely viscous with $\eta_{1M}/\eta_{2M}=10^2$ (second medium contribution substantial).

moderately small in Figs. 4(a) and 4(b) since $\beta_1/\beta_2=0.001$ which corresponds to $\eta_{1M}/\eta_{2M}\approx 10^6$, a lower limit for the case of a metal sample layer with water as the surrounding second medium. If the sample layer (medium 1) were behaving rigidly (simple added mass), $(R_m^s)_N$ would be only that contributed by the second medium (a constant), and $(X_m^s)_N$ would increase linearly with increasing $\beta_1 D$. As expected, Fig. 4(a) shows that $(R_m^s)_N$ is not zero, and that it exhibits a maximum when the layer 1 thickness is one fourth the shear wavelength ($\beta_1 D=1.57$). However, the range of this plot corresponds to larger sample layer thicknesses than are typical for QCMs as usually operated. [Although not shown here, there is an increased broadening and depression of this peak as β_1/β_2 increases (η_{2M}/η_{1M} increases), caused by the increased energy dissipation; thus increasing β_1/β_2 produces an even greater deviation from a simple mass-like impedance. Thus, $(R_m^s)_N$ becomes significant regardless of the value of α_1/β_1 as β_1/β_2 increases.][33]

A more typical range of sample layer thicknesses is that of Fig. 4(b); here a small but nonzero y intercept is observed, caused by the small but finite impedance of the second layer, which increases with increasing β_1/β_2. The closer the slope of the $(R_m^s)_N$ is to zero, the closer layer 1 mimics rigid behavior. The effect of medium 2 is seen in both the inset of Fig. 4(b) and in Fig. 4(c) where for very small medium 1 thicknesses $(R_m^s)_N$ is a function of α_1/β_1 and is independent of $\beta_1 D$ even if medium 1 is perfectly elastic ($\alpha_1/\beta_1=0$); $(R_m^s)_N$ also depends on α_2/β_2, of course.

The $(X_m^s)_N$ predictions for the conditions of Fig. 4 are shown in Fig. 5; in Figs. 5(a) and (b) the intercepts are nearly zero since $\beta_1/\beta_2=0.001$, and there is a nearly linear dependence of $(X_m^s)_N$ on $\beta_1 D$ for $\beta_1 D<0.3$ (slope depending on α_1/β_1). A linear dependence of $(X_m^s)_N$ on $\beta_1 D$ would correspond to rigid mass-like behavior of the sample layer as far as $(X_m^s)_N$ is concerned. The behavior of layers with $\alpha_1/\beta_1<0.4$ is markedly different when $\beta_1 D>0.6$, reminiscent of what was seen in the corresponding $(R_m^s)_N$ plots. Figure 5(b) illustrates predicted $(X_m^s)_N$ behavior for smaller $\beta_1 D$ values which correspond to more typical QCM operating conditions. The dependence of $(X_m^s)_N$ on $\beta_1 D$ is nearly linear for any α_1/β_1 value, and the slope depends on α_1/β_1; note that the slope depends on α_1/β_1 even when the sample layer exhibits rigid mass-like behavior because of the reduced variable ($\beta_1 D$) thickness format. Thus, when one calculates the impedance for a layer of specific thickness D for purely elastic and purely viscous cases, the $(X_m^s)_N$ values are very similar since when one changes the viscoelastic ratio (α/β) the specific value of β also changes. This is not directly reflected in these figures. Thus, for example, for a purely elastic sample layer ($\alpha_1/\beta_1=0.0$) with $D=5\,\mu$m, $f=5$ MHz, $\beta_1/\beta_2=0.001$, $\rho_1=\rho_2=1.0\,\mathrm{g/cm^3}$, and $\eta_{1M}=100P$, the $\beta_1 D=0.280$ and $(X_m^s)_N$ is 0.29 [■ on Fig. 5(b)]; if the same layer were purely viscous ($\alpha_1/\beta_1=1.0$), then $\beta_1 D=0.198$, and $(X_m^s)_N$ is 0.28 [◆ on Fig. 5(b)]. Thus for this specific case the maximum error in $(X_m^s)_N$ due to neglecting the viscoelastic ratio of layer 1 is about 3%. For larger β_1/β_2 this error will increase. For larger β_1/β_2 the y intercepts of $(X_m^s)_N$ vs. $\beta_1 D$ also become significant as the effects of the second medium become important; again they are a function of α_1/β_1 [see Fig. 5(c)] and α_2/β_2 (not shown). Similar behavior was seen for the intercepts for the $(R_m^s)_N$ plot [Fig. 4(c)]; however, the changes in the intercepts

Downloaded 19 Apr 2002 to 129.6.104.125. Redistribution subject to AIP license or copyright, see http://ojps.aip.org/jcpo/jcpcr.jsp

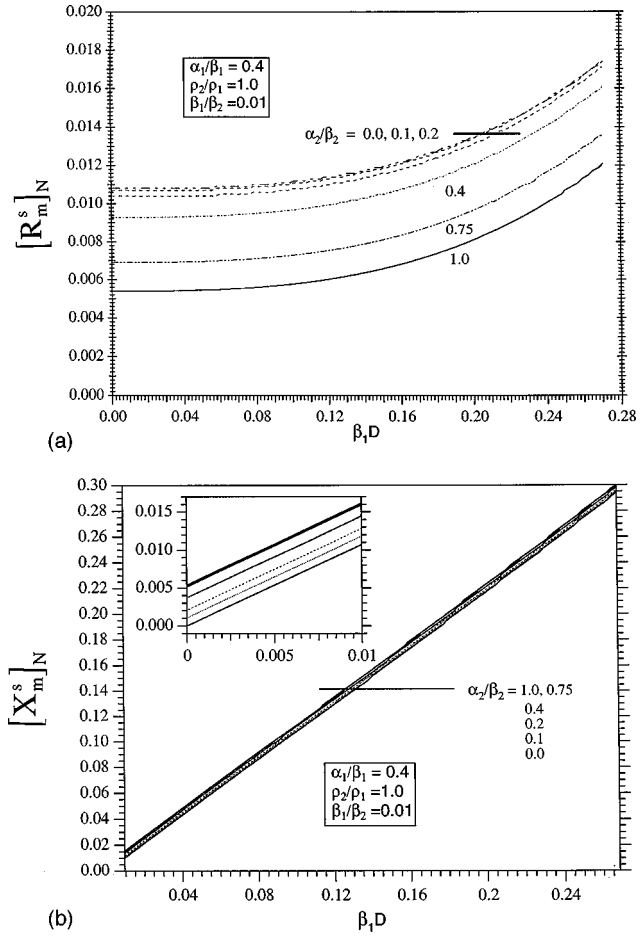

FIG. 6. (a) $(R_m^s)_N$ at $x=-D$ vs. $\beta_1 D$ for various values of α_2/β_2 for a small range of sample layer thickness; fairly elastic layer 1 with second medium of lower complex viscosity magnitude ($\eta_{1M}/\eta_{2M}=10^4$) (second medium contribution substantial). The effect of changing the ''viscoelastic ratio'' for layer 2 is shown. (b) $(X_m^s)_N$ at $x=-D$ vs. $\beta_1 D$ for various values of α_2/β_2 for a small range of sample layer thickness; fairly elastic layer 1 with second medium of lower complex viscosity magnitude ($\eta_{1M}/\eta_{2M}=10^4$) (second medium contribution modest). The effect of changing the ''viscoelastic ratio'' for layer 2 is shown.

for the $(X_m^s)_N$ curves of Fig. 5(c) are quite significant since $(X_m^s)_N$ directly affects the QCM resonance frequency. Thus these intercept shifts should be assessed for a specific experiment before employing simplified working equations for a QCM; the intercept is a function of β_1/β_2, α_1/β_1 (illustrated below), and α_2/β_2 so that knowledge of the mechanical properties of both layers may be necessary in order to determine the sample layer thickness.

The cases considered so far have assumed that medium 2 is purely viscous. The general impedance expression [Eq. (16)] enables for the first time an evaluation of the effect of a viscoelastic bath medium. To illustrate the effect of a viscoelastic second medium for representative values of the other variables, the case where α_1/β_1 is 0.4 and β_1/β_2 is 0.01 is shown. The focus is on small $\beta_1 D(\beta_1 D \leqslant 0.1)$, i.e., typical QCM conditions where one might expect Sauerbrey-type relations to hold. Figure 6(a) shows $(R_m^s)_N$ vs. $\beta_1 D$ for this specific case; changing the ''viscoelastic ratio'' α_2/β_2 of the second layer causes a substantial vertical shift [a nonzero $(R_m^s)_N$ is a deviation from an ideal mass-like impedance]. For $(X_m^s)_N$, shown in Fig. 6(b), there is again a vertical shift, which is a function of α_2/β_2; if the second medium is perfectly elastic, no vertical shift is seen in this range of $\beta_1 D$ (no shift in the QCM resonance frequency caused by bath medium). Thus, the contribution to $(X_m^s)_N$ from the second medium is dependent on the value of α_2/β_2. Note that in many cases this vertical shift could be determined experimentally from the difference in resonance frequency for the bare crystal vs. the crystal immersed in the second medium (no sample layer) if $\beta_1 D$ is sufficiently small. However, if the first layer is sufficiently thick or fairly lossy, this approach will not yield the correct offset frequency.

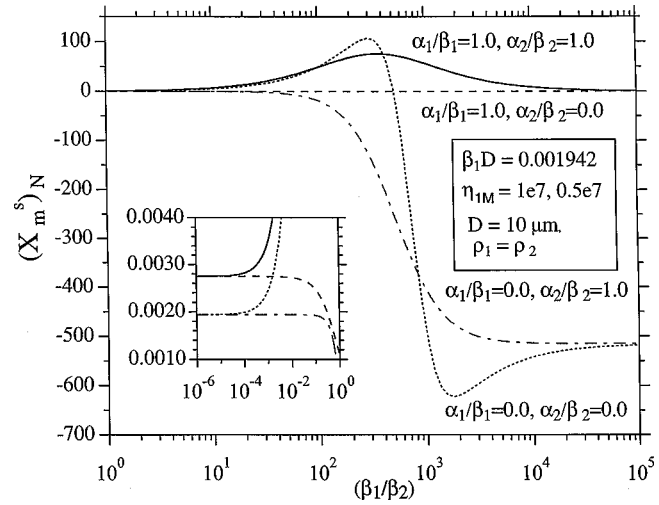

FIG. 7. Imaginary part $(X_m^s)_N$ of the reduced characteristic mechanical impedance at drive surface ($x=-D$) vs. $\beta_1/\beta_2(=\lambda_2/\lambda_1)$ for a specific case: $\beta_1 D=0.001\,942$, $D=10\ \mu$m, $\rho_1=\rho_2=1$ g/cm^3, $f_r^0=6\times10^6$ Hz. Curves shown correspond to limiting cases (viscous and elastic limits) for media 1 and 2. For viscous layer 1, $\eta_{1M}=5\times10^6 P$; for elastic layer 1, $\eta_{1M}=1\times10^7 P$. For small β_1/β_2, second medium has negligible effect; for intermediate (β_1/β_2), second medium has major influence that depends strongly on ''viscoelastic ratios'' of both sample and bath media.

Figure 6 illustrates a case where changing the viscoelastic properties (the ''viscoelastic ratio'' α_2/β_2) significantly affects the characteristic impedance; however, a different type of plot (Fig. 7) is needed to illustrate the transition from Sauerbrey-type to generalized impedance behavior, and also the extreme limiting behavior seen as η_{2M}/η_{1M} becomes very large. Figure 7 illustrates the remarkable changes in $(X_m^s)_N$ that occur as β_1/β_2 is varied (recall that $(\beta_1/\beta_2)=(\lambda_2/\lambda_1)=[(\rho_1/\rho_2)(\eta_{2M}/\eta_{1M})]^{1/2}\cdot\cos[(\pi/4)-(\phi_1/2)]/\cos[(\pi/4)-(\phi_2/2)]$) for a case where the layer 1 thickness is sufficiently small that Sauerbrey-type equations would apply if no second medium (bath) were present. The plots shown are for an operating frequency of 6 Mhz, a reduced layer 1 thickness $\beta_1 D=0.001\,942$, an actual layer 1 thickness $D=10\ \mu$m, and densities $\rho_1=\rho_2=1.00$ g/cm^3 for the four limiting cases for the viscoelastic properties of the two layers: both layers viscous $[(\alpha_1/\beta_1)=(\alpha_2/\beta_2)=1]$, both layers elastic $[(\alpha_1/\beta_1)=(\alpha_2/\beta_2)=0]$, layer 1 viscous with layer 2 elastic, $[(\alpha_1/\beta_1)=1,\ (\alpha_2/\beta_2)=0]$, and layer 1 elastic with layer 2 viscous $[(\alpha_1/\beta_1)=0,\ (\alpha_2/\beta_2)=1]$. (Note that the curves for which layer 1 is elastic are for $\eta_{1M}=1.0$

Downloaded 19 Apr 2002 to 129.6.104.125. Redistribution subject to AIP license or copyright, see http://ojps.aip.org/jcpo/jcpcr.jsp

$\times 10^7$ poise, and the curves for which layer 1 is viscous are for $\eta_{1M}=5\times 10^6$ poise to keep $\beta_1 D$ constant for all four cases.) Thus for this figure $(\beta_1/\beta_2)=(\eta_{2M}/\eta_{1M})^{1/2}\cdot[0.707 \text{ to } 1.414]$ so that $(\beta_1/\beta_2)^2$ is approximately equal to η_{2M}/η_{1M}. Thus this plot illustrates the onset of deviations from the simple Sauerbrey limit (left side of the figure) caused by the second medium as η_{2M}/η_{1M} becomes sufficiently large. The expanded-scale inset shows that the initial deviations from the Sauerbrey limit occur at very small β_1/β_2 values if layer 2 is viscous [$\approx$5% deviation in $(X_m^s)_N$ at $(\beta_1/\beta_2)=2\times 10^{-4}$, or $(\eta_{2M}/\eta_{1M})\approx 4\times 10^{-8}$]; if layer 2 is elastic, $\simeq$5% deviation in $(X_m^s)_N$ occurs at $\beta_1/\beta_2=4\times 10^{-2}$ if layer 1 is viscous and at $\beta_1/\beta_2=0.2$ if layer 1 is elastic. Thus knowledge of the ''viscoelastic ratio'' (α_2/β_2) for the second medium is crucial here in order to determine the sample layer thickness unless (β_1/β_2) is less than 10^{-4}. The behavior is more complicated than this might suggest, however. If η_{1M} is changed significantly, these curves shift in surprising ways. If layer 2 is viscous, the value of β_1/β_2 at which 5% deviation is seen shifts as $(\eta_{1M})^{1/2}$; if layer 2 is elastic, the 5% deviation point occurs at the same β_1/β_2 for all η_{1M} if η_{1M} is 1000 poise or greater.

From more extensive analyses of the characteristic impedance, it is evident that employing the usual simplified working equations introduces error, but this error is frequently negligibly small for many current QCM experiments. The magnitude of this error for specific experimental conditions being employed should be calculated before employing the simple working equations unless $\beta_1 D$ and β_1/β_2 are sufficiently small (see summary). Figures 3–7 demonstrate that knowledge of β_1/β_2 and the ''viscoelastic ratio'' for both layer 1 and layer 2 frequently are necessary to correctly determine sample layer thickness.

PREDICTION OF SAMPLE-INDUCED RESONANCE FREQUENCY SHIFTS FOR A SIMPLIFIED QCM MODEL

In the previous sections, expressions for the spatial variation of the medium velocity in either layer and the impedance sensed at the crystal surface have been presented. Although this impedance is experimentally accessible, it is not usually measured. To help provide a link to what is commonly measured (the resonance frequency shift due to media 1 and 2), we assume a simple harmonic oscillator model representation for the quartz crystal. Impedance expressions can then be employed to predict the change in resonance frequency that would be observed due to media 1 and 2.

In traditional applications of QCMs, the change in resonance frequency due to the sample and surrounding medium is measured. This shift is then analyzed assuming that the applied film is rigid, and that the effect of the surrounding medium is simply to cause a constant frequency shift that can be subtracted to obtain the frequency shift due only to the sample layer. Here the introduction of the simple harmonic oscillator (SHO) model of the QCM crystal makes it most convenient to evaluate the influence of the sample layer and surrounding bath medium on the resonance frequency in terms of actual sample thickness (μm) rather than the reduced variables format of Figs. 3–7; thus the frequency shift results are presented in a less universal but more recognizable format.

The use of SHO modeling of the crystal behavior represents a balance between mathematical tractability and detailed physical description. In this modeling there is no description of the spatial variation of the crystal displacement within the crystal, and no prediction of the mechanical Q to be expected for the bare crystal. However, predictions for much more complete physical models of the crystal itself are already available;[14] comparisons among existing theoretical predictions for physically realistic crystal models and the results for the simpler SHO crystal model presented here have been performed enabling a quantitative assessment of the small error associated with the SHO-based prediction of the QCM resonance frequency shifts induced by the sample and surrounding bath media. Two potential sources of small error when employing the SHO model are the shift in the nodal plane in the crystal with the addition of sample (layer 1) and surrounding medium if only one side of the crystal is loaded (this effect has been ignored since if both sides of the crystal are equally loaded, no nodal plane shift occurs), and the very small energy loss associated with the piezoelectric effect itself (also ignored). The negligibly small errors resulting from neglecting these effects are discussed later.

A simple harmonic oscillator picture has been applied to link the motion of the driving surface of the quartz resonator to the crystal resonance frequency and the mechanical impedance due to the sample layer and surrounding medium. The resonance frequency without sample, f_r^0, is given by

$$f_r^0=\frac{1}{2\pi}\sqrt{\frac{K}{M}}=\frac{1}{2h}\sqrt{\frac{G_q}{\rho_q}}, \tag{22}$$

where K is now the effective ''crystal spring constant'' which is approximately $(\pi^2/2)(G_qA)/h, G_q$ the shear modulus of quartz (3.09×10^{12} dynes/cm^2), A the crystal drive surface area, and h the thickness of the crystal ($h=0.108$ cm for 5 MHz crystals). M, the effective moving mass of the equivalent simple harmonic oscillator, is approximately $\rho_q Ah/2$, where ρ is the density (2.648 g/cm^3) of the quartz (assumes that the nodal plane of the quartz crystal is always at its geometric center; this is strictly correct only when both sides of the crystal are loaded identically). With sample and surrounding medium present, Eq. (22) becomes[52,45]

$$f_r=-\frac{AX_m^s}{4\pi M}+\sqrt{\left(\frac{AX_m^s}{4\pi M}\right)^2+(f_r^0)^2}, \tag{23}$$

where X_m^s is the imaginary component of the characteristic mechanical impedance due to the presence of the sample layer and surrounding bath medium. Thus $\Delta f_r\equiv f_r-f_r^0$ can be written as

$$\begin{aligned}\Delta f_r&=-\frac{f_r^0X_m^s}{\pi\sqrt{\rho_qG_q}}+\sqrt{\left(\frac{f_r^0X_m^s}{\pi\sqrt{\rho_qG_q}}\right)^2+(f_r^0)^2}-f_r^0\\&=-\frac{X_m^s}{2\pi\rho_qh}+\sqrt{\left(\frac{X_m^s}{2\pi\rho_qh}\right)^2+(f_r^0)^2}-f_r^0.\end{aligned} \tag{24}$$

Downloaded 19 Apr 2002 to 129.6.104.125. Redistribution subject to AIP license or copyright, see http://ojps.aip.org/jcpo/jcpcr.jsp

Equation (24) together with Eq. (18) for X_m^s enables calculation of Δf_r as a function of medium 1 thickness D (in cm), the α/β ratios for the two media, and the magnitude of the complex viscosity coefficients (in poise) for both media. Although Eq. (18) specifies Δf_r in terms of all five variables, in most applications the second (surrounding) medium has usually been a low viscosity, viscous fluid. For this reason the second medium is assumed to be a waterlike fluid for the example calculations shown.

To evaluate the precision of the SHO treatment of the crystal motion, comparisons with existing theoretical predictions based on more detailed models of the crystal have been performed. There are three analyses that are particularly useful: predictions for a crystal surrounded by a viscous medium, for a Sauerbrey type model of the same crystal with attached rigid layer, and for the crystal with an attached viscoelastic sample layer. The combination of Eqs. (24) and (18) reduces to known relations for the first two cases.[33]

The third and most thorough test of the present model is obtained by comparison with the detailed model of Kanazawa.[14] He evaluated the shear wave field within both the crystal resonator and an applied viscoelastic sample layer; the crystal is assumed to be perfectly elastic, and the piezoelectric properties of the quartz are explicitly included (produces a small increase in the shear modulus of the quartz). Thus his treatment rigorously models the behavior of the crystal and one applied sample layer; the two assumptions (no shift of nodal line position and no piezoelectric loss) employed in our treatment were not employed by Kanazawa.

Kanazawa denoted β/α as Q; he varied the β/α ratio for the sample layer by keeping G' constant and varying η' as needed to achieve a specific Q value.[14] He then obtained plots of Δf_r vs. D for a series of different Q values for layer 1. To facilitate comparisons between our results and those of Kanazawa, it is convenient to express α and β in terms of η' and G' rather than η_M and ϕ as in Eqs. (4) and (5). One obtains

$$\beta=\omega\sqrt{\frac{\rho}{2G'}}\frac{\left[\sqrt{1+\left(\frac{\omega\eta'}{G'}\right)^2}+1\right]^{1/2}}{\sqrt{1+\left(\frac{\omega\eta'}{G'}\right)^2}} \tag{25}$$

and

$$\alpha=\omega\sqrt{\frac{\rho}{2G'}}\frac{\left[\sqrt{1+\left(\frac{\omega\eta'}{G'}\right)^2}-1\right]^{1/2}}{\sqrt{1+\left(\frac{\omega\eta'}{G'}\right)^2}}. \tag{26}$$

Figure 8 illustrates the very good agreement obtained between Kanazawa's Δf_r predictions[14] and these of the present rigorous impedance analysis combined with our SHO-based approximate modeling of the crystal. Note that these plots are such that the wavelength of shear waves in the sample layer is different for each of the Q values plotted in Fig. 8. (To obtain this comparison Eqs. (18) and (24) were employed with η_2, $\rho_2 \Rightarrow 0$ so that $H^* \Rightarrow -1$.) Note that there are small but distinct discrepancies for small Q; these differences appear to be related to the nodal plane shift in the quartz (here only one side of the crystal was loaded). The smaller discrepancies for the large values of Q are possibly due to the piezoelectric stiffening effect. Thus, Fig. 8 gives confidence in the predictive validity (within 2% for Δf_r with one side loaded; within 0.5% with both sides loaded for $0.15 \leqslant D \leqslant 1$ μm) of the simple harmonic oscillator description of the quartz crystal surface motions.

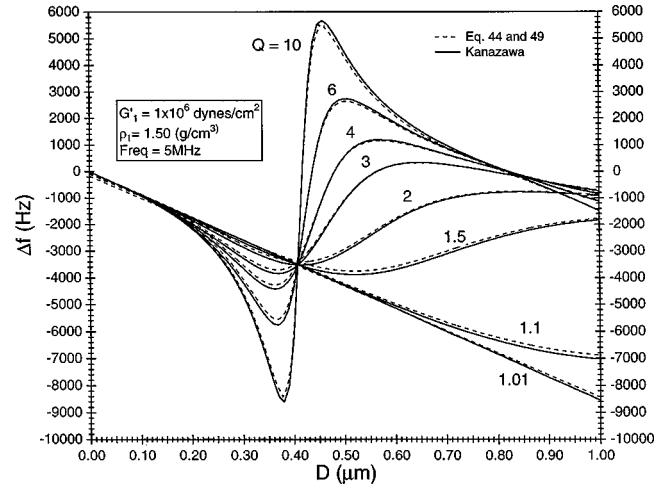

FIG. 8. Δf_r vs. D due to sample layer only (no layer 2). Kanazawa model: solid lines. Impedance/SHO model: dashed lines. Different Q values correspond to different sample properties and thus to different shear wavelengths in sample (see text).

The combination of the SHO-based model and the generalized characteristic mechanical impedance enables calculation of the Δf_r due to the sample layer and surrounding bath medium. Evaluation of Δf_r vs. D provides a third format for determining the range of Sauerbrey-type working equations. The major disadvantage of this format is that it requires specifying the physical properties of the sample layer and surrounding medium as well as various instrumental parameters; hence the predictions are specific to a particular set of experimental conditions. Here properties were selected that approximate many current experiments ($f_r^0 = 5$ MHz, $A = 0.317$ cm^2, $\alpha_2/\beta_2 = 1.0$, $\eta_{2M} = 0.01P$, $\rho_2 = \rho_1 = 1$ g/cm^3). Layer 1 thickness is in units of length (D) instead of wavelength ($\beta_1 D$).

Figure 9 illustrates the effect of changing the complex viscosity magnitude, η_{1M}, of the sample layer, assuming it to be perfectly elastic ($\alpha_1/\beta_1 = 0$); medium 2 is assumed to be purely viscous, with $\eta_{2M} = 0.01P$ (waterlike). Large deviations from simple mass-like behavior (Sauerbrey model; $\Delta f_r \propto D$) for layer 1 are apparent for thick layers when η_{1M} is lower than about 1000 P. Note that the deviations from Sauerbrey-type behavior occur at different specific D values for attached layers with different η_{1M} values, but the deviations begin at similar $\beta_1 D$ values. (Significant deviations occur at about 5 μm for the $\eta_{1M} = 100P$ case which corresponds to $\beta_1 D \cong 0.28$; for the $\eta_{1M} = 1000P$ case the same deviation occurs at about 12 μm or $\beta_1 D \cong 0.26$; these points are marked on the figure.)

Downloaded 19 Apr 2002 to 129.6.104.125. Redistribution subject to AIP license or copyright, see http://ojps.aip.org/jcpo/jcpcr.jsp

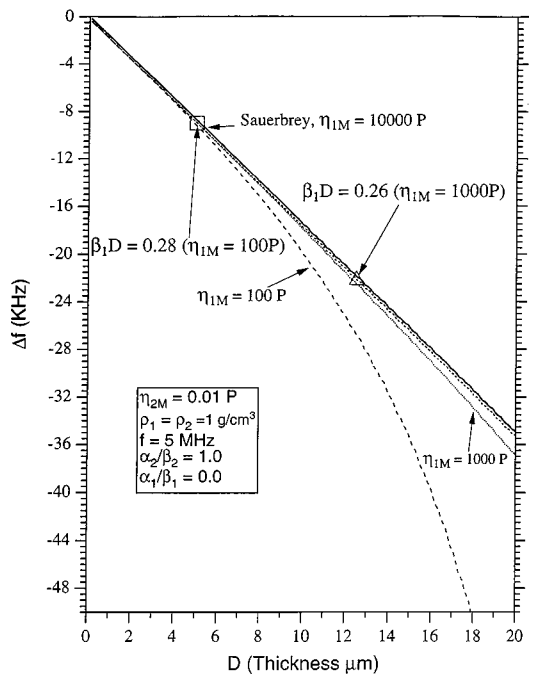

FIG. 9. Δf_r vs. D for perfectly elastic sample layer as function of η_{1M}. Medium 2 assumed water-like. Rigid layer (Sauerbrey) prediction shown as solid line. Onset of significant deviation from rigid layer behavior indicated for two cases: $\eta_{1M}=100P(\beta_1/\beta_2=0.0141)$, where deviation begins at $\beta_1 D\cong 0.28$; $\eta_{1M}=1000P(\beta_1/\beta_2=0.004\,47)$, where deviation begins at $\beta_1 D\cong 0.26$.

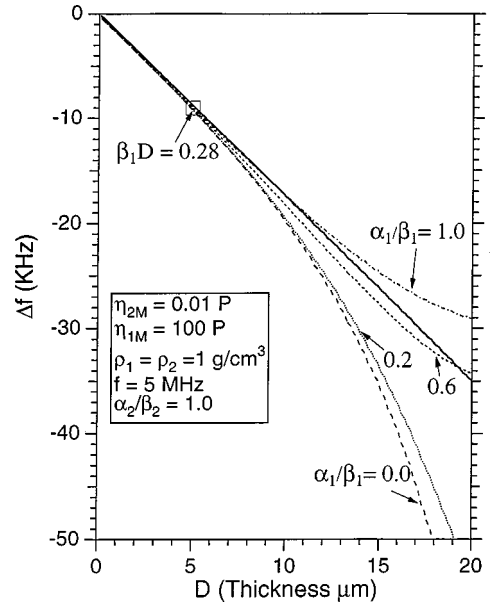

FIG. 10. Δf_r vs. D for sample layers with same η_{1M} but differing degrees of elastic behavior. Rigid layer (Sauerbrey) limit prediction also shown (solid line). Medium 2 assumed to be water-like.

Figure 10 illustrates deviations from simple rigid-layer behavior for sample layers with differing values of α_1/β_1. Again, medium 2 properties are waterlike. There is significant deviation for $\beta_1 D\geqslant 0.28$; values for the frequency shift that are greater than or less than that for rigid layer behavior (solid line) are observed depending on the value of α_1/β_1. Here it would be necessary to know the α/β ratios for both media and β_1/β_2 when assigning a thickness to the sample layer based on the frequency shift if $\beta_1 D$ is greater than about 0.06.

These representative plots of predicted Δf_r behavior only reflect changes in the resonance frequency, and thus in the imaginary component, X_m^s, of the characteristic impedance; in actual experiments the real component, R_m^s, will cause the observed motional resonance peak to broaden and the peak height to decrease in amplitude. If the drive electronics are such that the QCM is driven precisely at resonance, then X_m^s is readily determined from Δf_r. However, many QCM instruments employ simple electronic drive circuitry with high gain feedback loops so that piezoelectric noise voltage generates the initial drive signal; no drive oscillator is employed. Any feedback loop has an inherent finite time delay, so the instruments actually operate at an apparent resonance frequency slightly less than f_r. Thus the actual drive frequency is such that both X_m^s and R_m^s affect this apparent resonance frequency; if there is a change in R_m^s only, leading to a change in peak width but no change in f_r, an apparent resonance frequency shift would be measured. For example, a low frequency (13 kHz) QCM-type instrument being developed at NIST to detect the glassy-to-rubbery-state transition in a thin polystyrene sample layer showed an approximately 3 Hz shift in actual resonance frequency and a change in peak width (full width at half height) from about 2 to about 7 Hz as the sample went from the glassy to the rubbery state. If a drive circuit were employed in which the feedback loop was slow enough to introduce a 45 deg phase delay (exceptionally large phase shift), the apparent resonance frequency shift would be approximately 4.8 Hz as opposed to the actual resonance frequency shift of 3 Hz, leading to a value of X_m^s and sample layer thickness about 60% too large. Thus it is important that the QCM be operating at resonance for Eq. (24) to be valid.[45,52]

SUMMARY

Most theoretical modeling of QCM experiments has focused on extensive and more complete models of the crystal with varying degrees of rigor in treating the effect of an applied sample layer. This study concentrated on a rigorous description of the effect of an applied viscoelastic sample layer and surrounding viscoelastic bath medium, and then included the crystal by means of a somewhat simplified model. Since our results agree with the predictions from more complete descriptions of the crystal resonator to within two percent at worst, a straightforward and sufficiently accurate description of a QCM system including crystal, applied viscoelastic layer, and surrounding viscoelastic medium is now available, and experimentally verifiable predictions can be readily obtained. This allows for the assessment of error in the determination of sample layer thickness caused by various simplifications of the rigorous analysis equations presented here. Of particular interest is the assessment of the range of validity of the usual Sauerbrey-type analysis in which one assumes:

(a) $X_m^s=\omega\rho_1 D$ (Sauerbrey limit; no medium 2 present) so

Downloaded 19 Apr 2002 to 129.6.104.125. Redistribution subject to AIP license or copyright, see http://ojps.aip.org/jcpo/jcpcr.jsp

the Δf_r due to the sample layer is linearly related to the sample layer mass and hence its thickness;

(b) if a second (bath) medium is present, it produces a constant $\Delta f_r'$ offset independent of the sample layer thickness; this $\Delta f_r'$ offset is then subtracted from the measured total Δf_r to approximate the resonance frequency shift due to the sample layer.

Note that this assumes that the frequency shifts that would be seen for media 1 and 2 individually are simply additive when the two media are present simultaneously.

Extensive additional calculations (not shown) have been carried out in which parameters have been varied widely to cover the ranges in which QCMs might be employed [η_{1M} and η_{2M} from 10^2 to 10^9 poise, β_1/β_2 from 10^{-6} to 10^{11}, D up to 20 μm, f_r from 1 to 6 MHz, $\rho_1=\rho_2=1.0\,\mathrm{g/cm^3}$, and α_1/β_1 and α_2/β_2 varied independently between 0 (elastic limit) and 1 (viscous limit)]. From these results it is clear that if $\beta_1 D$ is sufficiently small [$(\beta_1 D)\leqslant 0.0628$, or $(D/\lambda)\leqslant 0.01$ so that one would be in the Sauerbrey limit if only layer 1 were present], and β_1/β_2 is sufficiently small [limiting values are $(\beta_1/\beta_2)\leqslant 0.04$ if layer 1 is viscous; $(\beta_1/\beta_2)\leqslant 0.2$ if layer 2 is elastic], then X_m^s for the QCM with sample layer 1, immersed in bath medium 2 is, to a good approximation (less than five percent error), equal to the sum of the individual contributions (usual assumption). Thus in this regime

$$X_m^s \cong (X_m^s)_{s,1}+(X_m^s)_2 \cong \omega\rho_1 D+\sqrt{\omega\rho_2\eta_{2M}}\sin[(\pi/4)-(\phi_2/2)], \tag{27}$$

and the resultant Δf_r is given by

$$\Delta f_r \simeq (\Delta f_r)_{s,1}+(\Delta f_r)_2 \simeq -\frac{\sqrt{f_r^0}}{\rho_q h}\left\{\sqrt{f_r^0}\rho_1 D+\sqrt{\frac{\rho_2\eta_{2M}}{2\pi}}\sin[(\pi/4)-(\phi_2/2)]\right\}, \tag{28}$$

where the subscripts s, 1 denote Sauerbrey limit for layer 1, and 2 denotes bath medium 2. Also, note that in this regime one does not need to know the viscoelastic properties of either medium since the Sauerbrey limit for layer 1 is independent of these properties and the medium 2 contribution can be measured directly by simply immersing the bare crystal in medium 2.

However, if either $\beta_1 D>0.0628$ or β_1/β_2 exceeds the limits specified (>0.04 if layer 1 is viscous; >0.2 if layer 1 is elastic), the simple additivity assumption fails and one must use the rigorous X_m^s of the characteristic impedance [Eq. (18)] together with Eq. (24) to obtain Δf_r for a given layer thickness D, or D for a given Δf_r. Thus, here one must know or measure (at f_r^0) the viscoelastic properties of both media in order to obtain D from a measured Δf_r.

A further simplification results when $\beta_1 D\leqslant 0.0628$ and β_1/β_2 is sufficiently small ($\leqslant 0.04$ if layer 1 is viscous; $\leqslant 0.2$ if layer 1 is elastic) and the second (bath) medium is such that

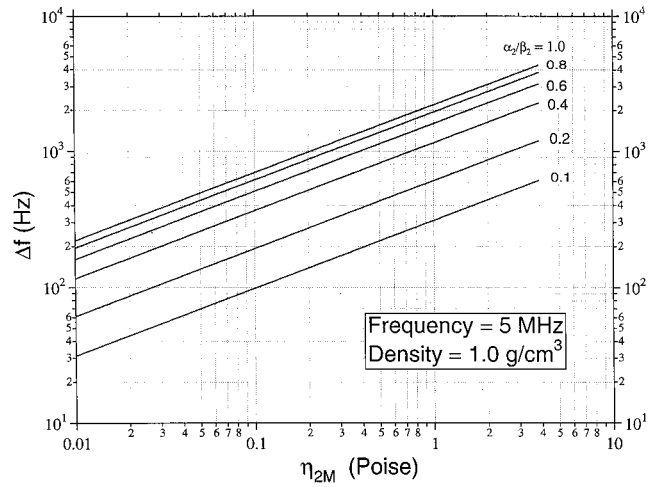

FIG. 11. Δf_r vs. η_{2M} for second medium (infinite in extent); there is no layer 1. The effect of changing α_2/β_2 is explored, illustrating that the frequency shift due to medium 2 is a function of both η_{2M} and the ''viscoelastic ratio'' for the bath medium.

$$\eta_{2M}\leqslant 1.57\times 10^5\cdot\frac{\rho_1^2}{\rho_2}\cdot D^2 \quad \text{(cgs units)}, \tag{29}$$

(D in cm); then the second medium contribution can be ignored (less than three percent error). Note, however, that for sufficiently thin films even the correction for air or partial vacuum (nearly same η_{2M}) becomes essential. Figure 11 shows the Δf_r due to shear wave propagation in medium 2 (no sample layer present) as functions of η_{2M} and α_2/β_2, which corresponds to $(\Delta f_r)_2$ when the criteria for simple additivity of the independent frequency shifts are met.

It is clear that the second (bath) medium in many QCM experimental situations has produced an effectively independent Δf_r shift. However, care should be exercised when considering QCM applications to new samples to insure that this assumption is valid. The theoretical predictions of three different aspects of the QCM experiment (the spatial variation of the velocity, the characteristic mechanical impedance due to sample layers, and the Δf_r) taken together show the physical basis for observed deviations from Sauerbrey-like behavior. Of these, the impedance is probably the most useful since full impedance measurements would result in more information than is currently obtained from Δf_r data.

ACKNOWLEDGMENTS

Partial financial support was provided by the Polymers Program of the Division of Materials Research of the National Sciences Foundation (Grants DMR-9223212 and DMR-9818585) and by the Graduate Research Committee of the Graduate School of the University of Wisconsin-Madison.

APPENDIX: EVALUATION OF PARTICLE VELOCITY AND VELOCITY GRADIENT IN MEDIA 1 AND 2

From Eqs. (7) and (8) the spatial variation of the velocity $\dot{\xi}^*$ in medium 1 is given by

Downloaded 19 Apr 2002 to 129.6.104.125. Redistribution subject to AIP license or copyright, see http://ojps.aip.org/jcpo/jcpcr.jsp

$$\dot{\xi}^* = \overline{\mathrm{A}} e^{+i(\omega t - \gamma_1 x)} + \overline{\mathrm{B}} e^{+i(\omega t + \gamma_1 x)}, \quad \text{for} \quad -D \leqslant x \leqslant 0 \tag{A1}$$

and in medium 2 by

$$\dot{\xi}^* = \overline{\mathrm{C}} e^{+i(\omega t - \gamma_2 x)}, \quad \text{for} \quad x \geqslant 0. \tag{A2}$$

From Equation (9) and the assumed coordinate system, the shear rate $\dot{\gamma}^*_{xy} = \partial \dot{\xi}_y / \partial x = g^*$, the velocity gradient in the x direction.

The three unspecified complex coefficients $(\overline{\mathrm{A}}, \overline{\mathrm{B}}, \overline{\mathrm{C}})$ in Eq. (A1) and (A2) are evaluated by employing three boundary conditions: no slip at the interfaces at $x = -D$ and $x = 0$, and shear stress continuity across the $x = 0$ interface. Thus

$$\dot{\xi}^*|_{x=-D} = \xi_0 e^{i\omega t}, \tag{A3}$$

$$\dot{\xi}^*_1|_{x=0} = \dot{\xi}^*_2|_{x=0}, \tag{A4}$$

and

$$\eta^*_1 g^*_1|_{x=0} = \eta^*_2 g^*_2|_{x=0}. \tag{A5}$$

A useful quantity, H^*, that appears in subsequent equations is defined as

$$H^* \equiv \frac{\eta^*_2 \gamma_2 - \eta^*_1 \gamma_1}{\eta^*_2 \gamma_2 + \eta^*_1 \gamma_1} = \frac{-\dfrac{\rho_2 \gamma_1}{\rho_1 \gamma_2} + 1}{-\dfrac{\rho_2 \gamma_1}{\rho_1 \gamma_2} - 1}. \tag{A6}$$

Application of the boundary conditions to Eqs. (A1) and (A2) yields

$$\overline{\mathrm{A}} = \frac{\dot{\xi}_0}{e^{i\gamma_1 D} - H^* e^{-i\gamma_1 D}}, \tag{A7}$$

$$\overline{\mathrm{B}} = -\frac{\dot{\xi}_0 H^*}{e^{i\gamma_1 D} - H^* e^{-i\gamma_1 D}}, \tag{A8}$$

$$\overline{\mathrm{C}} = \frac{\dot{\xi}_0 (1 - H^*)}{e^{i\gamma_1 D} - H^* e^{-i\gamma_1 D}}. \tag{A9}$$

Substituting these expressions into Eqs. (A1) and (A2) give

$$\dot{\xi}^* = \frac{\dot{\xi}_0 (e^{-i\gamma_1 x} - H^* e^{i\gamma_1 x}) e^{i\omega t}}{e^{i\gamma_1 D} - H^* e^{-i\gamma_1 D}} \quad \text{for} \quad -D \leqslant x \leqslant 0, \tag{A10}$$

and

$$\dot{\xi}^* = \frac{\dot{\xi}_0 (e^{-i\gamma_2 x} - H^* e^{i\gamma_2 x}) e^{i\omega t}}{e^{i\gamma_1 D} - H^* e^{-i\gamma_1 D}} \quad \text{for} \quad x \geqslant 0. \tag{A11}$$

The velocity gradient is obtained from Eqs. (A10), (A11), and (9).

$$g^* = -\frac{\dot{\xi}_0 (i\gamma_1 e^{-i\gamma_1 x} + H^* i\gamma_1 e^{-i\gamma_1 x}) e^{i\omega t}}{e^{i\gamma_1 D} - H^* e^{-i\gamma_1 D}} \quad \text{for} \quad -D \leqslant x \leqslant 0, \tag{A12}$$

and

$$g^* = \frac{\dot{\xi}_0 (-i\gamma_2 e^{-i\gamma_2 x} + H^* i\gamma_2 e^{-i\gamma_2 x}) e^{i\omega t}}{e^{i\gamma_1 D} - H^* e^{-i\gamma_1 D}} \quad \text{for} \quad x \geqslant 0. \tag{A13}$$

Equations (A10)–(A13) specify the velocity and velocity gradient in each of the two media. In order to examine the predictions of these expressions it is convenient to rewrite them in terms of real and imaginary components. Consider the H^* parameter from Eq. (A6); since $\gamma_j = \beta_j - i\alpha_j$, γ_1/γ_2 can be written as

$$\frac{\gamma_1}{\gamma_2} = \frac{\beta_1 [1 + (\alpha_1/\beta_1)^2]^{1/2}}{\beta_2 [1 + (\alpha_2/\beta_2)^2]^{1/2}} e^{-i[\tan^{-1}(\alpha_1/\beta_1) - \tan^{-1}(\alpha_2/\beta_2)]} = A e^{-i\theta}, \tag{A14}$$

so that H^* can be written as

$$H^* = \frac{[(\rho_2/\rho_1)A]^2 - 1 - i[2(\rho_2/\rho_1)A \sin\theta]}{[(\rho_2/\rho_1)A]^2 + 2(\rho_2/\rho_1)A \cos\theta + 1} = c + id. \tag{A15}$$

The expressions for the velocity and velocity gradient profiles may now be written out more simply. To do so, eight additional useful quantities are defined as follows:

$$K \equiv (1+c)\cos(\beta_1 x)\cosh(\alpha_1 x) - d\sin(\beta_1 x)\cosh(\alpha_1 x) + (c-1)\cos(\beta_1 x)\sinh(\alpha_1 x) - d\sin(\beta_1 x)\sinh(\alpha_1 x), \tag{A16}$$

$$L \equiv (1+c)\sin(\beta_1 x)\sinh(\alpha_1 x) + d\cos(\beta_1 x)\sinh(\alpha_1 x) + (c-1)\sin(\beta_1 x)\cosh(\alpha_1 x) + d\cos(\beta_1 x)\cosh(\alpha_1 x), \tag{A17}$$

$$E \equiv (1-c)\cos(\beta_1 D)\cosh(\alpha_1 D) - d\sin(\beta_1 D) \times \cosh(\alpha_1 D) + (c+1)\cos(\beta_1 D)\sinh(\alpha_1 D) + d\sin(\beta_1 D)\sinh(\alpha_1 D), \tag{A18}$$

$$F \equiv (1+c)\sin(\beta_1 D)\cosh(\alpha_1 D) + (1-c)\sin(\beta_1 D) \times \sinh(\alpha_1 D) + d\cos(\beta_1 D)\sinh(\alpha_1 D) + d\cos(\beta_1 D)\cosh(\alpha_1 D), \tag{A19}$$

$$P \equiv (1-c)\cos(\beta_1 x)\cosh(\alpha_1 x) + d\sin(\beta_1 x)\cosh(\alpha_1 x) - (c+1)\cos(\beta_1 x)\sinh(\alpha_1 x) + d\sin(\beta_1 x)\sinh(\alpha_1 x), \tag{A20}$$

$$Q \equiv (1+c)\sin(\beta_1 x)\cosh(\alpha_1 x) - (1-c)\sin(\beta_1 x) \times \sinh(\alpha_1 x) + d\cos(\beta_1 x)\sinh(\alpha_1 x) + d\cos(\beta_1 x)\cosh(\alpha_1 x), \tag{A21}$$

$$J \equiv (c-1)\cos(\beta_2 x)\cosh(\alpha_2 x) - d\sin(\beta_2 x)\cosh(\alpha_2 x) + (c-1)\cos(\beta_2 x)\sinh(\alpha_2 x) - d\sin(\beta_2 x)\sinh(\alpha_2 x), \tag{A22}$$

Downloaded 19 Apr 2002 to 129.6.104.125. Redistribution subject to AIP license or copyright, see http://ojps.aip.org/jcpo/jcpcr.jsp

$$N \equiv -(c-1)\sin(\beta_2 x)\sinh(\alpha_2 x) - d\cos(\beta_2 x)\sinh(\alpha_2 x) + (c-1)\sin(\beta_2 x)\cosh(\alpha_2 x) - d\cos(\beta_2 x)\cosh(\alpha_2 x). \tag{A23}$$

With these definitions, Eqs. (A10) and (A12) can be rewritten as

$$\dot{\xi}^* = \frac{\dot{\xi}_0[P-iQ]}{[E+iF]} e^{i\omega t} = \frac{\dot{\xi}_0[P^2+Q^2]^{1/2}}{[E^2+F^2]^{1/2}} e^{i[\omega t - \tan^{-1}(Q/P) - \tan^{-1}(F/E)]} \quad \text{for } -D \leqslant x \leqslant 0, \tag{A24}$$

and

$$g^* = -\frac{\dot{\xi}_0 i\gamma_1[K+iL]e^{i\omega t}}{[E+iF]} = \frac{\dot{\xi}_0\beta_1[1+(\alpha_1/\beta_1)^2]^{1/2}[K^2+L^2]^{1/2}}{[E^2+F^2]^{1/2}} \times e^{i[\omega t - \pi/2 - \tan^{-1}(\alpha_1/\beta_1) - \tan^{-1}(L/K) - \tan^{-1}(F/E)]} \quad \text{for } -D \leqslant x \leqslant 0. \tag{A25}$$

The equivalent expressions for medium 2 are obtained by rewriting Eqs. (A11) and (A13).

$$\dot{\xi}^* = \frac{\dot{\xi}_0[J+iN]}{[E+iF]} e^{i\omega t} = \frac{\dot{\xi}_0[J^2+N^2]^{1/2}}{[E^2+F^2]^{1/2}} e^{i[\omega t + \tan^{-1}(N/J) - \tan^{-1}(F/E)]} \quad \text{for } x \geqslant 0, \tag{A26}$$

and

$$g^* = \frac{\dot{\xi}_0 i\gamma_2[J+iN]e^{i\omega t}}{[E+iF]} = \frac{\dot{\xi}_0\beta_1[1+(\alpha_1/\beta_1)^2]^{1/2}[J^2+N^2]^{1/2}}{[E^2+F^2]^{1/2}} \times e^{i[\omega t + \pi/2 - \tan^{-1}(\alpha_1/\beta_1) + \tan^{-1}(N/J) - \tan^{-1}(F/E)]} \quad \text{for } x \geqslant 0. \tag{A27}$$

These expressions have been checked against two well-known limits. First, if medium 2 is set to a very high viscosity, then the general expressions must reduce to the ''fixed reflector'' case.[46,49]

If the viscosity of medium 2 is such that $|\eta_2^*| >>> |\eta_1^*|$, then $H^* \Rightarrow 1$, and Eqs. (A24) and (A25) reduce to

$$\dot{\xi}^* = \frac{\dot{\xi}_0(e^{-i\gamma_1 x} - e^{i\gamma_1 x})e^{i\omega t}}{e^{i\gamma_1 D} - e^{-i\gamma_1 D}} \quad \text{for } -D \leqslant x \leqslant 0, \tag{A28}$$

and

$$g^* = -\frac{\dot{\xi}_0(i\gamma_1 e^{-i\gamma_1 x} + i\gamma_1 e^{+i\gamma_1 x})e^{i\omega t}}{e^{i\gamma_1 D} - e^{-i\gamma_1 D}} \quad \text{for } -D \leqslant x \leqslant 0, \tag{A29}$$

which are the known expressions for the fixed reflector geometry.[46,49] Second, if the properties of the two media are identical, the velocity and velocity gradient expressions must reduce to those for a freely propagating plane shear wave traveling in the $+x$ direction since no reflected waves will be produced at $x=0$. Setting $\eta_2^* = \eta_1^*$ gives $H^*=0$, and Eqs. (A24) and (A25) reduce to

$$\dot{\xi}^* = \frac{(\dot{\xi}_0 e^{-i\gamma_1 x})e^{i\omega t}}{e^{+i\gamma_1 D}} \quad \text{for } x \geqslant -D, \tag{A30}$$

and

$$g^* = -\frac{\dot{\xi}_0(i\gamma_1 e^{-i\gamma_1 x})e^{i\omega t}}{e^{i\gamma_1 D}} \quad \text{for } x \geqslant -D, \tag{A31}$$

which are the expected freely propagating shear wave expressions.[46,47,49]

[1] G. G. Guilbault and J. M. Jordan, Crit. Rev. Anal. Chem. **19**, 1 (1988).
[2] C. K. Barker and J. R. Reynolds, J. Electroanal. Chem. **251**, 307 (1988).
[3] K. H. Behrndt, J. Vac. Sci. Technol. **8**, 622 (1971).
[4] S. Bruckenstein, R. R. McCaffrey, and P. N. Prasad, Langmuir **2**, 228 (1986).
[5] R. P. Buck, E. S. Grabbe, and D. R. Melroy, J. Electroanal. Chem. **223**, 67 (1987).
[6] D. A. Buttry and M. R. Deaking, Anal. Chem. **61**, 1147a (1989).
[7] C. C. Day and A. G. Forton, Thermochim. Acta **103**, 75 (1986).
[8] J. F. Evans, D. M. Ullevig, and G. Albrecht, Anal. Chem. **54**, 2241 (1982).
[9] E. L. Fuller and K. A. Thomson, Langmuir **3**, 699 (1987).
[10] J. G. Gordon and K. K. Kanazawa, Anal. Chem. **57**, 1770 (1985).
[11] J. G. Gordon and K. K. Kanazawa, Anal. Chim. Acta **175**, 99 (1985).
[12] W. D. Hinsberg and K. K. Kanazawa, Rev. Sci. Instrum. **60**, 489 (1989).
[13] D. Johannsmann, K. Mathauer, G. Wegner, and W. Knoll, Phys. Rev. B **46**, 7808 (1992).
[14] K. K. Kanazawa and O. R. Melroy, IBM J. Res. Dev. **37**, 157 (1993).
[15] R. D. Kaiser, L. Reinisch, and J. Krim, Phys. Rev. Lett. **63**, 1743 (1989).
[16] M. M. Lien, M. Naoi, and W. H. Smyri, J. Electroanal. Chem. **272**, 273 (1989).
[17] M. Lindsröm and M. Laatikanen, J. Colloid Interface Sci. **125**, 610 (1988).
[18] D. C. Loveday, A. R. Hillerman, and S. Bruckenstein, Langmuir **7**, 191 (1991).
[19] C. Lu and O. Lewis, J. Appl. Phys. **44**, 4385 (1972).
[20] C. Lu and A. W. Czanderna, in *Methods and Phenomena*, edited by S. P. Wolsky (Elsevier, Amsterdam, 1984), Vol. 7.
[21] J. J. McCallum, Analyst (Cambridge, U.K.) **114**, 1173 (1989).
[22] H. Muramatsu, E. Tamiya, and I. Karube, Anal. Chim. Acta **215**, 91 (1988).
[23] R. Schumacher, Angew. Chem. **29**, 329 (1990).
[24] M. Shay and S. Bruckenstein, Electrochim. Acta **30**, 1295 (1985).
[25] D. H. Solina, J. Krim, and R. Chiarello, Phys. Rev. Lett. **66**, 181 (1991).
[26] H. Terashima, J. Colloid Interface Sci. **125**, 444 (1988).
[27] P. T. Varineau and D. A. Buttry, J. Phys. Chem. **91**, 1292 (1987).
[28] C. G. Willson, W. D. Hinsberg, and K. K. Kanazawa, J. Electrochem. Soc. **133**, 1448 (1986).
[29] M. Okuhara and T. Normura, Anal. Chim. Acta **142**, 281 (1982).
[30] G. Sauerbrey, Physik Verhandl. **8**, 113 (1957).
[31] G. Sauerbrey, Z. Phys. **155**, 206 (1959).
[32] Z. Lin and M. Ward, Anal. Chem. **67**, 685 (1995).
[33] C. C. White, Ph.D. thesis, University of Wisconsin-Madison, 1994.
[34] W. G. Cady, *Piezoelectricity, An Introduction to the Theory and Applications of Electromechanical Phenomena in Crystals* (Dover, New York, 1946).
[35] W. P. Mason, *Physical Acoustics and the Properties of Solids* (Van Nostrand, New York, 1958)

Downloaded 19 Apr 2002 to 129.6.104.125. Redistribution subject to AIP license or copyright, see http://ojps.aip.org/jcpo/jcpcr.jsp

[36] W. P. Mason, *Piezoelectric Crystals and Their Application to Ultrasonics* (Van Nostrand, New York, 1950)
[37] M. D. Ward and D. A Buttry, Science **249**, 1000 (1990)
[38] M. Onoe, Proc. IRE **45**, 694 (1957).
[39] C. Stockbridge, *Vacuum Microbalance Techniques* (Plenum, New York, 1966)
[40] J. G. Miller and D. I. Bolef, J. Appl. Phys. **39**, 4589 (1968).
[41] E. Benes and H. Nowotny, J. Acoust. Soc. Am. **82**, 513 (1987).
[42] E. Benes, J. Appl. Phys. **56**, 608 (1984).
[43] E. Nwankwo and C. J. Durning, Rev. Sci. Instrum. **69**, 2375 (1998).
[44] R. A. Crane and G. Fischer, J. Phys. D: Appl. Phys. **12**, 2019 (1979).
[45] J. D. Ferry, *Viscoelastic Properties of Polymers*, 3rd ed. (Wiley, New York, 1980).
[46] J. L. Schrag, Trans. Soc. Rheol. **21**, 399 (1977).
[47] G. B. Thurston and J. L. Schrag, J. Appl. Phys. **35**, 144 (1964).
[48] G. B. Thurston and J. L. Schrag, J. Chem. Phys. **45**, 3373 (1966).
[49] J. L. Schrag, J. F. Guess, and G. B. Thurston, J. Appl. Phys. **36**, 1996 (1965).
[50] R. B. Bird, R. C. Armstrong, and O. Hassager, *Dynamics of Polymeric Liquids*, Volume 1. Fluid Mechanics, 2nd ed.; and Volume 2. Kinetic Theory, 2nd ed. (Wiley, New York, 1987)
[51] J. L. Schrag and G. Woltman (unpublished); F. I. Braid, Ph.D. thesis, University of Wisconsin-Madison, 1996.
[52] J. L. Schrag and R. M. Johnson, Rev. Sci. Instrum. **42**, 224 (1971).
[53] C. Zener, *Elasticity and Anelasticity of Metals* (University of Chicago Press, Chicago, 1948)
[54] R. Lakes, *Viscoelastic Solids* (CRC, Cleveland, Ohio, 1998)

Downloaded 19 Apr 2002 to 129.6.104.125. Redistribution subject to AIP license or copyright, see http://ojps.aip.org/jcpo/jcpcr.jsp